JMEPEG (2010) 19:714–720
DOI: 10.1007/s11665-009-9533-4

1059-9495/$19.00

Fracture Toughness of Heat-Treated Superaustenitic Stainless Steels

C. Muller and L. Scott Chumbley

(Submitted March 31, 2009; in revised form June 22, 2009)

Cast duplex and superaustenitic stainless steels are attractive alloys for applications that desire high strength and high corrosion resistance. Due to the large amounts of alloying additions present in these systems, a proper solution heat-treatment schedule is critical in ensuring that the alloys are able to meet the desired specifications. While studies to determine the phase transformation behavior of duplex and superaustenitic alloys have shown that the precipitation kinetics are comparatively slow when considering large amounts of precipitation, studies involving Charpy impact specimens have noted significant decreases in impact strength in materials improperly heat treated for times as short as 10 min, well before any significant amount of precipitation (<1 vol.%) has occurred. The goal of this study was to investigate a particular superaustenitic alloy, CN3MN, in an effort to determine the reason for this large drop in impact strength. Charpy impact specimens were tested from polycrystalline and single crystal samples in the solution heat-treated condition and after heat treatment at 872 °C for times ranging from 5 to 60 min to embrittle the material. Fracture surfaces were characterized using optical and scanning electron microscopy (SEM), Auger spectroscopy, and energy dispersive x-ray spectroscopy. The fracture surfaces showed ductile and brittle characteristics for the standard and improperly treated samples, respectively. Close observation using SEM reveals precipitation takes place initially on grain boundaries, which may account for the observed embrittling effect. While difficult to see at very short times, measurements of linear coverage of precipitation along grain boundaries of polished samples show a definite relationship between drop in fracture toughness and grain boundary precipitation. The results of the Charpy tests and SEM observations, along with chemical analysis studies of the grain boundaries using x-rays and auger electrons, will be presented.

Keywords failure analysis, heat treating, stainless steels, superalloys

1. Introduction

Superaustenitic and duplex stainless steels are specifically designed to produce excellent pitting and crevice corrosion resistant properties at high temperatures and in seawater by a controlled blend of alloying additions. The major alloying additions are Cr, Mo, and Ni, but Si, Cu, Mn, W, and N to lesser extents are also common, which can cause the balance amount of Fe to be less than 50% of the total in the superaustenitic alloys. Given the large amount of alloying additions, it is not surprising that extended use at elevated temperatures results in precipitation of a number of second phases, including carbides, nitrides, and intermetallic phases (Ref 1-4). The most commonly observed secondary phases include $M_{23}C_6$ carbide, and intermetallic sigma, chi, and Laves phases (Ref 1-4), although other phases such as M_6C, π, R, and Cr_2N have been seen, depending on the particular alloy and heat treatment carried out (Ref 1-4).

C. Muller and **L. Scott Chumbley**, Department of Materials Science and Engineering, Iowa State University, Ames, IA. Contact e-mail: chumbley@iastate.edu.

Studies to determine the transformation kinetics of certain duplex and superaustenitic steels (Ref 5-9) have shown that the specific precipitate that forms is a function of the local composition as well as heating time and temperature. The intermetallic compounds σ, χ, and Laves dominate in terms of overall volume percent of precipitation. The rates of nucleation and subsequent growth have been observed to vary widely depending on the specific alloy and heat treatment considered. For example, in studies of the superaustenitic alloy CK3MCuN, precipitation of σ is seen in solution-treated samples in times as short as 1 min in the temperature range of 700 to 800 °C. However, subsequent nucleation (accompanied by growth) of σ is so sluggish that the volume percent of second phase does not reach 5% until 8000 min have passed at 800 °C, with times even longer at lower temperatures. Increase of the temperature to 900 °C increases σ nucleation times to 10 min; however, nucleation of χ in addition to σ results in 5 vol.% of overall precipitation being reached after only 300 min.

It is well known that formation of second phases can cause a decrease in the mechanical properties and corrosion resistance of highly alloyed steels (Ref 1, 2, 4, 5). For this reason, ASTM A923 Methods A, B, and C have been developed as a means of detecting the presence of intermetallics that may be detrimental to the mechanical properties and corrosion performance of cast duplex alloys (Ref 10-12). Studies have shown that the impact toughness of the duplex alloys is extremely sensitive to small amounts of precipitation. Similarly, a recent study of superaustenitic steels has shown a significant drop in absorbed energy after relatively short-term anneals at high temperature (Ref 13).

Thus, it appears that these highly alloyed systems are less dependent on total precipitation volume percentages than they are on specific factors concerning the nature of the initial precipitation. Possible factors related to this unexpected drop in fracture toughness might include location of the precipitation (e.g., does it occur along grain boundaries), type of precipitation (e.g., is it an embrittling sulfide or intermetallic), and shape (e.g., acicular or spheroidal). Some initial observations using transmission electron microscopy of superaustenitic steels noted preferential precipitation along some grain boundaries (Ref 9), suggesting grain boundary embrittlement as a likely cause.

The purpose of this article is to examine precipitation behavior in a cast superaustenitic steel, particularly in regard to the initial formation of secondary phases. Efforts were concerned with producing samples where the fracture toughness was seen to drop, followed by characterization of the fracture surfaces using optical and electron microscopy, with special consideration paid to grain boundaries. The alloy examined was the cast superaustenitic alloy CN3MN, and samples were examined in both the solution heat-treated condition and solution heat treated plus a subsequent embrittling heat treatment. These results will be discussed in light of reported deterioration of fracture toughness.

2. Experimental Procedure

Material from a single heat of CN3MN in the form of $3 \times 4 \times 35$ cm^3 keel bars was received from a collaborating foundry in the as-solution heat-treated condition. All keel bars came from sand castings and had been heat treated between 1160 and 1230 °C for 2 h. Nominal composition for the material obtained in weight percent was C ≈ 0.23, Si ≈ 0.74, Mn ≈ 0.59, P ≈ 0.013, S ≈ 0.004, Cr ≈ 20.9, Mo ≈ 6.5, Ni 24.6, Cu ≈ 0.12, and N ≈ 0.22. Charpy impact samples 1 cm × 1 cm × 5.5 cm were machined from the keel blocks at various locations and then subsequently subjected to further solution heat treatments at 1200 °C for 3 h. Samples for embrittlement were heated to 872 °C for times ranging from 5 min to 1 h, followed by an air cool. For all heat treatments, samples were encapsulated in quartz under an argon atmosphere, and placed in a box furnace. The impact samples were tested using a Tinius-Olsen Impact tester with a maximum energy of 407 J at a temperature of −40 °C.

Using a portion of the same polycrystalline keel bar for starting material, a single crystal of CN3MN was grown using the facilities of the Materials Preparation Center (Ref 14). The single crystal was grown using the Bridgeman Method, the result being roughly cylindrical in shape, approximately 7 cm in length and 4 to 5 mm in diameter. This crystal was used to prepare four smaller Charpy impact specimens (Fig. 1). The dimensions of these samples were 1/2 those of the full-sized samples, resulting in 1/4 the volume being present. These samples received the same solution heat treatment as the full-size specimens. The quartz on one of the specimens broke during the solution treatment and was exposed to oxygen, causing a slight discoloration. This sample and another one were embrittled using the same heat treatment described above. The impact samples were tested using a bench top Tinius-Olsen Impact tester with a maximum energy of 19 J at room temperature and at −40 °C. (N.B. The actual energy applied using this unit was measured electronically based on pendulum swing arc so that samples that did not fracture but deformed would display an absorbed energy less than the maximum.)

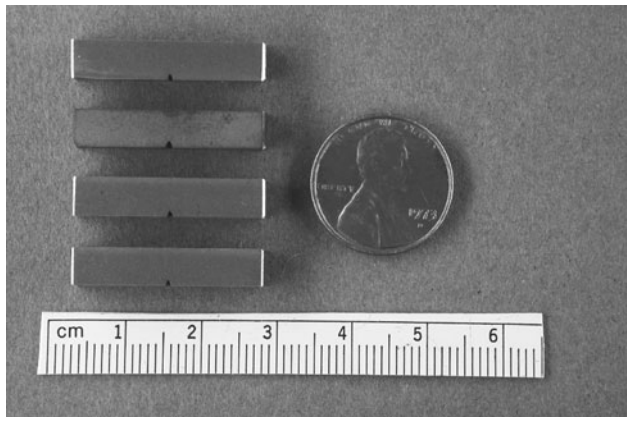

Fig. 1 Single crystal Charpy specimens. Second sample from top exhibited slight oxidation after solution heat treatment

Fracture surfaces and polished samples prepared using standard metallographic techniques were characterized using a scanning electron microscope (SEM) equipped with an x-ray energy dispersive spectrometer (EDS) for chemical analysis. A JEOL Auger spectrometer equipped with an in situ fracture stage was also employed to study fracture surfaces that were exposed when samples were broken under the high vacuum conditions of the Auger.

3. Experimental Results

3.1 Charpy Impact Results

The Charpy impact results obtained from polycrystalline material are shown in Fig. 2. For comparison, the data from the earlier study by Siewert et al. (Ref 13) are also shown. Note that the properly heat-treated samples withstood the impact and did not completely fracture, even at the test temperature of −40 °C. This was also true for a single sample that was erroneously notched on both sides of the test bar.

Samples that had undergone the embrittling heat treatment showed a significant drop in fracture toughness (Fig. 2b) as noted by other studies (Ref 10-13). Although a single sample tested at room temperature exhibited a higher fracture toughness than those tested at −40 °C, the drop in toughness was still remarkable and easily identified.

Impact strength as a function of heat treatment time at 872 °C is shown in Fig. 3. A significant drop in toughness is seen after times as short as 15 min. A slight difference is seen between samples tested at room temperature or −40 °C, the former having almost twice the impact strength as the latter. It should be noted that the sample used for the 60 min aging experiments tested at −40 °C had a slightly higher average impact strength (34 J as opposed to 17 J) than the specimens tested in Fig. 2.

When the single crystal samples were tested, all samples withstood the test without breaking or cracking, yielding a consistent maximum of 11 J. The deformation produced in the

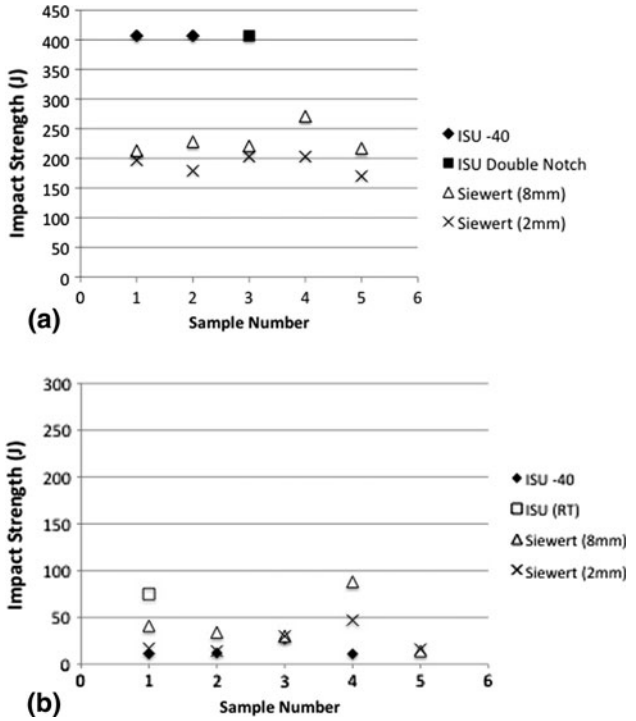

Fig. 2 (a) Charpy impact results for properly solution heat-treated CN3MN. (b) Charpy impact results for improperly solution heat-treated CN3MN

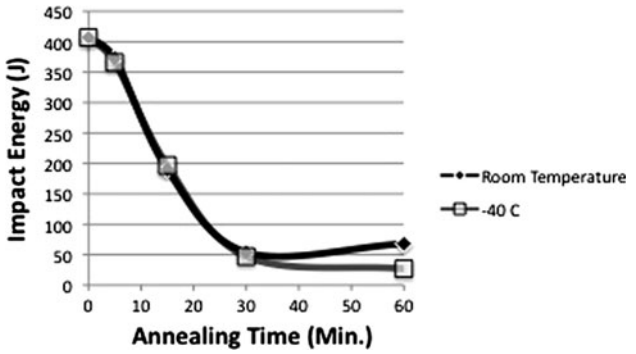

Fig. 3 Impact strength as a function of time-at-temperature for an 872 °C heat treatment

test pieces is approximately the same for all conditions, as shown in Fig. 4. The deformation for the solution heat-treated sample tested at −40 °C was slightly larger; however, this sample absorbed multiple strikes before the pendulum could be secured. For comparison, the fracture of a similar-sized mild carbon steel sample is included.

One might question whether the applied load was sufficient for an adequate test. Considering the data from Fig. 2(b), full-sized embrittled samples required an energy of approximately 17 J to fracture at −40 °C; this was somewhat higher for the results shown in Fig. 3 where the average was ≈34 J. If one assumes a 1/4 reduction in required energy for the smaller-sized samples due to the 1/4 reduced volume, at most an impact strength of 7 to 8 J was expected. This value is well below the maximum energy absorbed by the samples.

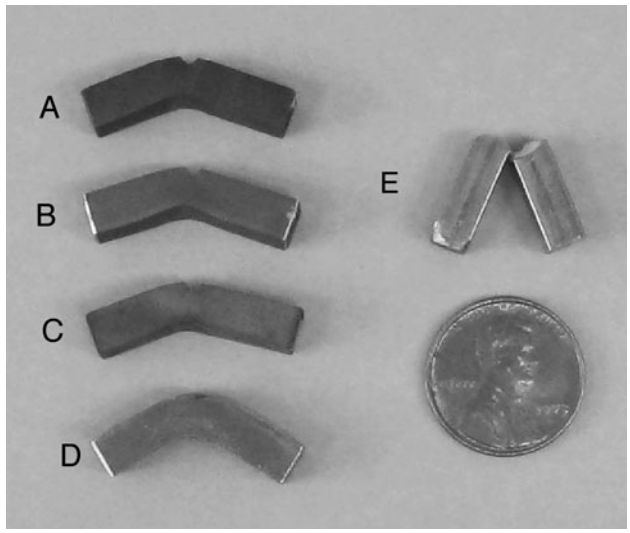

Fig. 4 Single crystal impact samples. (A) Embrittled sample accidentally exposed to oxygen, room temperature test; (B) solution heat treated, room temperature; (C) embrittled, −40 °C test; (D) solution heat treated, −40 °C (multiple strikes); and (E) a mild carbon steel sample fractured at room temperature for comparison

3.2 Fracture Surface Examination

Examples of the fracture surfaces obtained for both good and embrittled material are shown in Fig. 5. The embrittled material shows clear signs of intergranular fracture at low magnification (Fig. 5b), while the properly treated material shows classic dimpled fracture at high magnifications (Fig. 5c). Evidence of grain boundary precipitation is observed in the embrittled material at higher magnification; however, it is difficult to determine whether the contrast exhibited by the grain surfaces are due to simple cleavage or fracture of a thin precipitate layer that might be covering the grain surface (Fig. 5d).

The mode of fracture observed and the evidence of grain boundary precipitation implies grain boundary embrittlement, most likely due either to segregation of harmful elements (e.g., S) to the grain boundaries or precipitation of thin brittle phases (e.g., sigma, chi, Laves) on all of the grain surfaces.

3.3 Grain Boundary Precipitation

SEM micrographs of polished samples corresponding to samples heat treated at 872 °C are shown in Fig. 6. It is difficult to determine in the earliest stages (5 and 15 min) whether precipitation is present on the grain boundary as a thin layer. Some discrete particles appear to be forming after 15 min and can clearly be resolved after 30 min.

The contrast exhibited by the precipitates visible at longer times is consistent with phases higher in Cr and/or Mo than the surrounding matrix; the small size of the precipitates prevented any conclusions being drawn as to whether one or two different types of precipitates were present, as had been seen in other studies which examined heat-treated CN3MN samples (Ref 8, 9).

The result of an EDS line scan using the SEM is shown in Fig. 7. The extremely small size of the precipitates makes quantitative analysis impossible. However, it can be said that the precipitates and possibly the grain boundary region are

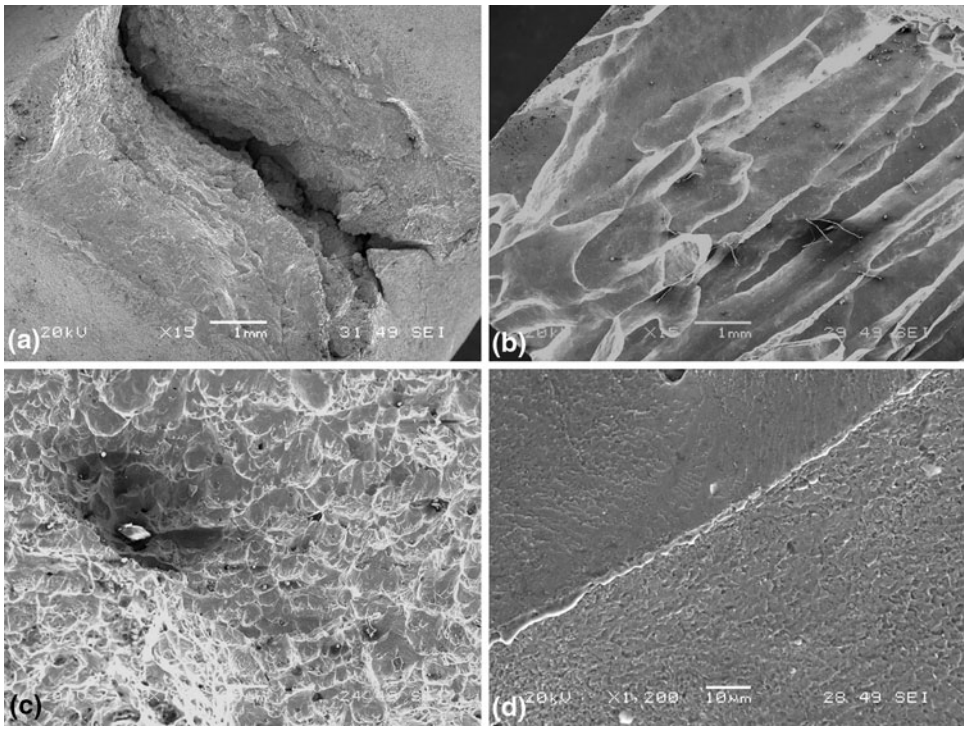

Fig. 5 SEM images of (a) properly solution treated material and (b) embrittled material taken at low magnification. High magnification shows (c) classic dimple fracture for properly treated materials. (d) Evidence of grain boundary precipitation in embrittled materials

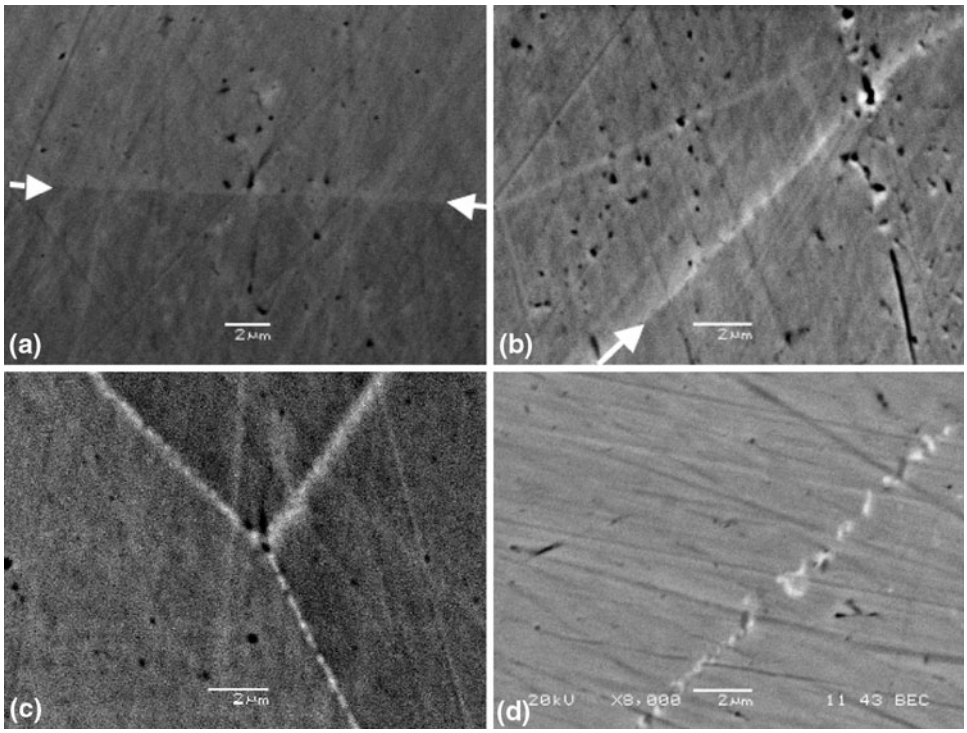

Fig. 6 Polished SEM images of solution heat-treated CN3MN that was subsequently heat treated at 872 °C for (a) 5 min; (b) 15 min; (c) 30 min; and (d) 1 h. Arrows show the position of the grain boundary

enriched in Cr and Mo and possibly S. Overlap of the S K_α and Mo L_α peaks used for analysis make it difficult to say if S is present, and the fact that the S scan follows the trace of the Mo scan extremely well makes the S data suspect. While the Cr and Mo enrichment appears slight in the line scan analysis, it must be remembered that spreading of the electron beam into the

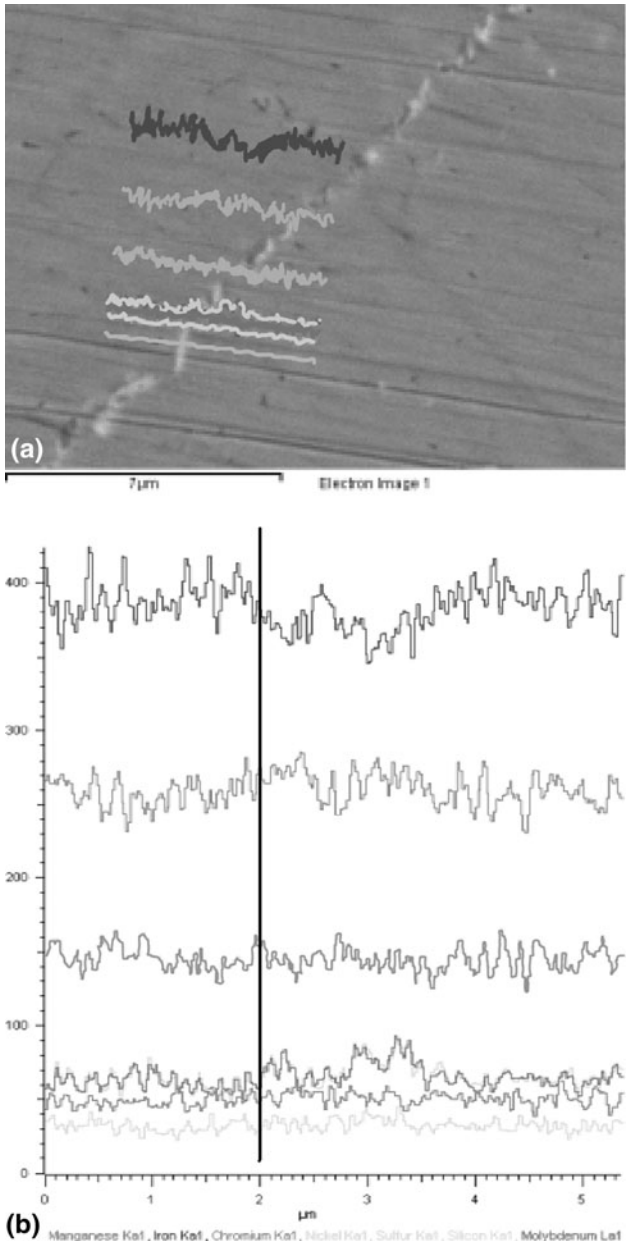

Fig. 7 Analysis of grain boundary composition using EDS. (a) Region showing from where the data was obtained. (b) The data obtained. Grain boundary shown by thick line. A slight enrichment in Cr and Mo is seen

surrounding matrix will result in a dilution of the heavier Cr and Mo elements being measured (Ref 15).

In an effort to conclusively determine whether Mo or S (or both) was segregating to the grain boundary, Auger analysis was used. Auger analysis has the additional advantage of being surface sensitive, allowing qualitative chemical composition analysis of fractured grain boundaries to be conducted essentially at the boundary surface, eliminating the beam spreading effects and subsurface sampling inherent in EDS. When used in conjunction with an ion sputtering gun, composition profiles could be obtained starting at the sample surface and moving into the grain interior.

For these studies, small impact samples were fractured in situ within the Auger spectrometer at liquid nitrogen

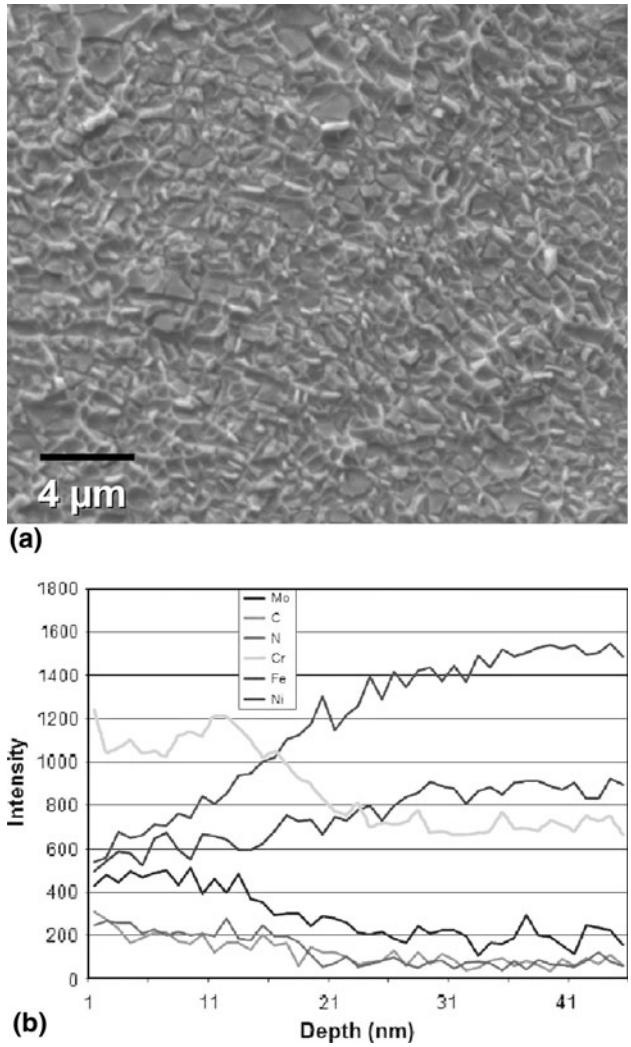

Fig. 8 Auger spectrometer results. (a) Secondary electron image of a grain surface and (b) Composition depth profiles obtained from embrittled CN3MN

temperatures. Incorrectly heat-treated samples fractured very easily and grain surfaces were readily available. A typical grain surface imaged using secondary electrons is shown in Fig. 8(a). This surface appears to consist of small, fractured precipitates.

A typical composition depth profile obtained from a grain surface is shown in Fig. 8(b). Significant Cr and Mo enrichment is seen, with no evidence of S segregation. In fact, the S signal was so low as to not register as even being present. This suggests that the EDS results showing sulfur are entirely due to Mo L_α x-rays rather than S K_α radiation. The Cr and Mo enrichment extends to a depth of 20 to 40 nm before reaching equilibrium values.

4. Discussion

The full-size Charpy impact tests verified that severe embrittlement occurred in polycrystalline samples that were heat treated at 872 °C for 1 h. Tests conducted where the material was embrittled at 872 °C for various times show a drop in fracture toughness that corresponds with the appearance

Table 1 Linear percentage of grain boundary coverage

Annealing time, min	Grain boundary coverage (linear percentage, %)
5	$\approx 0 \pm 8$
15	$\approx 33 \pm 8$
30	60 ± 5
60	65 ± 5

of precipitation on the grain boundaries. Charpy tests at room temperature and at −40 °C, which both show embrittlement, show that the effect is relatively independent of test temperature.

Smaller test samples obtained from a single crystal grown from the same composition and subjected to the same heat treatment conditions showed no difference in impact strength, with all the samples sustaining the strike of the hammer without fracturing or cracking. These results prove conclusively that the drop in fracture toughness is associated with a grain boundary precipitation effect.

Detailed examination of CN3MN showed that precipitation was evident on the grain boundaries after relatively short periods of time, and it is believed that this is directly responsible for the large drop seen in fracture toughness of these materials. Linear percentages (distance along the grain boundary covered by precipitation/unit distance) quantifying the apparent grain boundary coverage were obtained from the images shown in Fig. 6, and these values are given in Table 1. It should be noted that all the measurements cited contain a great deal of uncertainty, especially at the shorter times of 5 and 15 min where low signal and small precipitate size require a considerable amount of judgment to be made as to whether a precipitate is, in fact, present. Given these difficulties, there is a good correspondence between measured linear coverage and the drop in impact strength seen in Fig. 3, and this relationship is shown graphically in Fig. 9.

X-ray and Auger studies show increased Cr and Mo in the grain boundary region, but the small size scale of the precipitates that are observed prevent unambiguous determination of the second phase or phases. While S was also detected at the grain boundaries using EDS, this observation was not confirmed using Auger analysis, and it is believed that the S signal obtained using x-rays was a false reading due to the overlap that exists between the S K_α and the Mo L_α x-ray peaks. While S is a well-known cause of grain boundary embrittlement, and a small amount could be present which can not be detected easily using EDS and might even be missed using Auger electrons, at this time there is no conclusive evidence that S segregation is taking place.

The submicron size of the precipitates seen in these early stages prevented the exact nature of the precipitate to be determined. In a previous study, TEM observation of samples heat treated at 900 °C revealed initial precipitation along grain boundaries at overall volume percentages no greater than 1 vol.% (Ref 9). Two different precipitates with different crystal structures were observed in this previous study with approximate compositions that could be related to sigma, chi, or Laves phase formation, depending on local equilibrium.

Since all possible intermetallics in the system are brittle, the key factor in determining the onset of the observed drop in fracture toughness appears to be less concerned with the exact nature of the precipitate than in determining the point at which a significant fraction of the boundary becomes decorated with intermetallic precipitation. However, identification of the initial precipitate that forms may be key in designing an alloy that is resistant to this rapid and harmful precipitation.

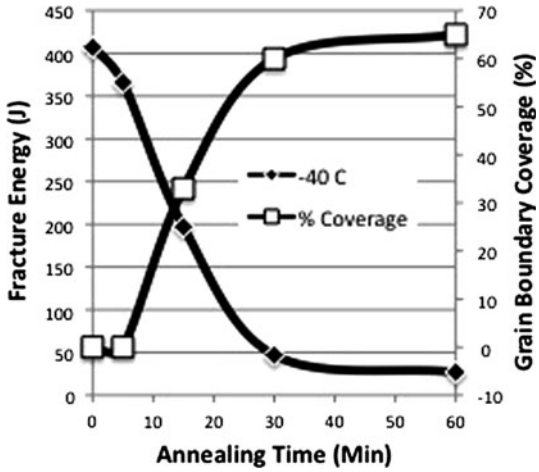

Fig. 9 Correlation between drop in fracture toughness and increase of grain boundary precipitation coverage

5. Summary and Conclusions

The superaustenitic stainless steel CN3MN was heat treated and tested under conditions corresponding to properly solution heat treated and embrittled. Charpy impact tests run on the samples produced showed that the fracture toughness dropped drastically after the improper heat treatment of 872 °C for 1 h, the failure mode being intergranular cleavage. The noted embrittlement occurred well before any significant amounts of precipitation had occurred in the sample as predicted by recently developed transformation diagrams. Characterization of the fracture surfaces using SEM and a combination of x-ray EDS and Auger spectroscopies revealed extremely small precipitates on the grain boundaries that are enriched in Mo and Cr. Although the small size scale of the precipitates prevented conclusive identification, they are assumed to be either sigma or Laves phase, which were the intermetallics observed to first precipitate in CN3MN in previous studies.

Acknowledgments

This work was funded by the United States Department of Energy through a grant administered by the American Institute of Technology, and was in collaboration with the Steel Founders' Society of America (SFSA), the John Deere Technology Center, Stainless Foundry, Allegheny Ludlum, Southern Steel, ANCAST, Keokuk Steel Castings, MetalTek, Lehigh University, Wollaston Alloy Inc., AG Anderson, Nova Precision Castings Corp, and Talladega Castings & Machine. The authors are especially thankful to Malcolm Blair and Ron Bird for helpful discussions. This work was performed at Ames Laboratory and Iowa State University.

References

1. S. Heino, Role of Mo and W During Sensitization of Superaustenitic Stainless Steel—Crystallography and Composition of Precipitates, *Metall. Mater. Trans. A*, 2000, **31**, p 1893–2904
2. S. Heino, M. Knutson-Wedel, and B. Karlsson, Precipitation in High Nitrogen Superaustenitic Stainless Steel, *Mater. Sci. Forum*, 1999, **318–320**, p 143–148
3. M. Svoboda, A. Kroupa, J. Soousek, J. Vrest'al, and P. Miodownik, Phase Changes in Superaustenitic Steels After Long-Term Annealing, *Z. Metallkd.*, 2004, **95**, p 1025–1030
4. T.-H. Lee, S.-J. Kim, and Y.-C. Jung, Crystallographic Details of Precipitates in Fe-22Cr-21Ni-6Mo-(N) Superaustenitic Stainless Steels Aged at 900°C, *Metall. Mater. Trans. A*, 2000, **31**, p 1713–1723
5. Y.-J. Kim, L.S. Chumbley, and B. Gleeson, Determination of Isothermal Transformation Diagrams for Sigma-Phase Formation in Cast Duplex Stainless Steels, *Met. Trans. A*, 2004, **35**, p 3377–3386
6. Y.-J. Kim, O. Ugurlu, C. Jiang, B. Gleeson, and L.S. Chumbley, Microstructural Evolution of Secondary Phases in the Cast Duplex Stainless Steels CD3MN and CD3MWCuN, *Met. Trans.*, 2007, **38**(2), p 203–211
7. Y.-J. Kim, L.S. Chumbley, and B. Gleeson, Continuous Cooling Transformation in Cast Duplex Stainless Steels CD3MN and CD3MWCuN, *J. Mater. Eng. Perform.*, 2008, **17**, 32
8. N.S.L. Phillips, L.S. Chumbley, and B. Gleeson, Determination of Isothermal Diagrams for Sigma and Chi Phase Formation in Superaustenitic Stainless Steels, *Technical and Operating Conference*, Nov 2–5, 2005, Steel Founders Society of America, Chicago, IL, 2005
9. N. Phillips, L.S. Chumbley, B. Gleeson, and O. Ugurlu, Determination of Phase Transformations in Cast Superaustenitic Stainless Steels, *Technical and Operating Conference*, Dec 14-16, 2006, Steel Founders Society of America, Chicago, IL, 2006
10. C. Lundin, Y. Cai, and V. Hariraran, Duplex Castings Perform equivalent to Wrought Material for Mechanical Properties and Corrosion Behavior, *Proceedings of the International Conference & Expo (Duplex 2007)*, June 18-20, 2007 (Grado, Italy), 2007
11. C. Lundin and S. Russell, "Detecting the Presence of Intermetallic Phases in Cast Duplex Stainless Steel," Report to Steel Founders Society of America, 2003
12. C. Lundin, S. Wen, and W. Ruprecht, Corrosion, Toughness, Weldability, and Metallurgical Evaluation of Cast Duplex Stainless Steels, *Proceedings of International Duplex America 2000 Conference*, Feb 29-Mar 1, 2000 (Houston, TX), 2000
13. T. Siewert, B. Siewert, and R. Santoyo, "Effect of CVN Striker Radius on Absorbed Energy and Lateral Expansion for Various Stainless Steels," Report to ASTM Committee, unpublished research, 2006
14. Single crystal synthesized at the Materials Preparation Center, Ames Laboratory, USDOE. See www.mpc.ameslab.gov
15. J. Goldstein, D. Newbury, P. Echlin, D. Joy, A. Romig, C. Lyman, C. Fiori, and E. Lifshin, *Scanning Electron Microscopy and X-ray Microanalysis*, Plenum Press, New York, 1992